Available online at www.sciencedirect.com
ScienceDirect
New Astronomy Reviews 50 (2006) 925–931
New Astronomy Reviews
www.elsevier.com/locate/newastrev

ARCADE: Absolute radiometer for cosmology, astrophysics, and diffuse emission ☆

A. Kogut [a,*], D. Fixsen [a,b], S. Fixsen [a,b], S. Levin [c], M. Limon [a,b], L. Lowe [a,b], P. Mirel [a,b], M. Seiffert [c], J. Singal [d], P. Lubin [d], E. Wollack [a]

[a] *NASA Goddard Space Flight Center, Code 685, Greenbelt, MD 20771, United States*
[b] *Science Systems and Applications, Inc., Goddard Space Flight Center, Code 665, Greenbelt, MD 20771, United States*
[c] *Jet Propulsion Laboratory, Pasadena, CA, United States*
[d] *University of California at Santa Barbara, CA, United States*

Abstract

The absolute radiometer for cosmology, astrophysics, and diffuse emission (ARCADE) is a balloon-borne instrument designed to measure the temperature of the cosmic microwave background at centimeter wavelengths. ARCADE searches for deviations from a blackbody spectrum resulting from energy releases in the early universe. Long-wavelength distortions in the CMB spectrum are expected in all viable cosmological models. Detecting these distortions or showing that they do not exist is an important step for understanding the early universe. We describe the ARCADE instrument design, current status, and future plans.

Keywords: Cosmology; Cosmic microwave background; Instrumentation

Contents

1. Introduction

The cosmic microwave background has proven to be an invaluable probe of physical conditions in the early universe. Temperature anisotropy in the CMB records the density and gravitational potential at an epoch when the fluctuations leading to the present-day large scale structure

☆ This work was supported by the suborbital program of the NASA Science Mission Directorate under RTOP 188-02-54-01.
* Corresponding author.
E-mail address: alan.j.kogut@nasa.gov (A. Kogut).
URL: http://arcade.gsfc.nasa.gov/ (A. Kogut).

1387-6473/$ - see front matter © 2006 Elsevier B.V. All rights reserved.
doi:10.1016/j.newar.2006.09.023

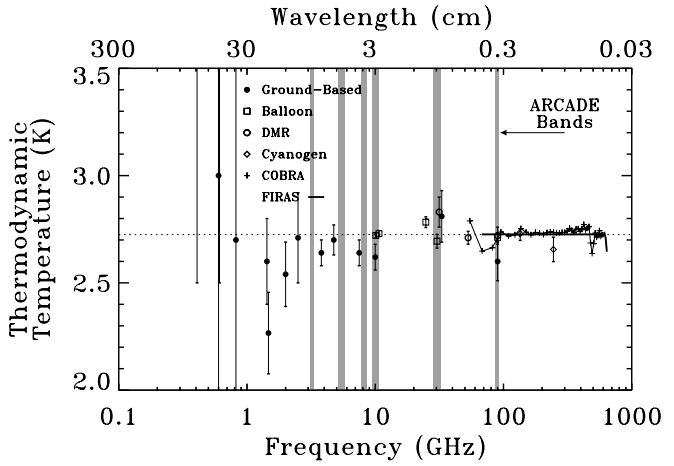

Fig. 1. Precise measurements of the CMB thermodynamic temperature. The dotted line represents a blackbody spectrum. The gray bands show the ARCADE frequencies. The CMB spectrum is poorly constrained at centimeter or longer wavelengths.

were still in the linear regime. The CMB spectrum, by contrast, provides information on the energetics, including the critical period after recombination when the currently-observed large-scale structures first formed. Precise measurements of the CMB spectrum provide important information on the early universe.

The frequency spectrum of the cosmic microwave background (CMB) carries a history of energy transfer between the evolving matter and radiation fields in the early universe. Energetic events (particle decay, star formation) heat the diffuse matter which then cools via interactions with the background radiation, distorting the radiation spectrum away from a blackbody. The amplitude and shape of the resulting distortion depend on the magnitude and redshift of the energy transfer (Zeldovich and Sunyaev, 1969; Burigana et al., 1991; Burigana et al., 1995).

Measurements across the peak of the CMB spectrum limit deviations from a blackbody to less than 50 parts per million (Mather, 1990; Gush et al., 1990; Fixsen and Mather, 2002). Direct observational limits at longer wavelengths, however, are weak: distortions as large as 5% could exist at wavelengths of several centimeters or longer without violating existing observations (Fig. 1). Plausible physical processes are expected to generate observable distortions without violating limits established at shorter wavelengths. Free-free emission from reionization and subsequent structure formation adds photons to the diffuse background, creating a spectral distortion $\Delta T_{\rm ff} = T_\gamma Y_{\rm ff}/x^2$, where T_γ is the undistorted photon temperature, x is the dimensionless frequency $h\nu/kT_\gamma$,

$$Y_{\rm ff} = \int_0^z \frac{k[T_{\rm e}(z) - T_\gamma(z)]}{T_{\rm e}(z)} \frac{8\pi e^6 h^2 n_{\rm e}^2 g}{3m_{\rm e}(kT_\gamma)^3\sqrt{6\pi m_{\rm e} kT_{\rm e}}} \frac{{\rm d}t}{{\rm d}z'}{\rm d}z', \quad (1)$$

is the optical depth to free-free emission, and g is the Gaunt factor (Bartlett and Stebbins, 1991). The distorted CMB spectrum is characterized by a quadratic rise in temperature at long wavelengths. The amplitude of the free-free signal depends on the column $\int n_{\rm e}^2$ of ionized gas and thus on the redshift $z_{\rm r}$ at which the first collapsed objects formed. Such a distortion must exist, with predicted amplitude of a few mK at frequency 3 GHz (Haiman and Loeb, 1997; Gnedin and Ostriker, 1997; Oh, 1999). Detection of the free-free distortion would place important constraints on the era of luminous object formation and the extent of clumping in galactic halos.

The decay of massive particles or other relics produced near the big bang will also distort the CMB spectrum. Energy released at an early epoch to either charged particles or photons will heat free electrons, which then cool via compton scattering from the colder CMB photons. For energy released at redshift $z < 10^4$ the gas is optically thin, resulting in a uniform decrement $\Delta T_{\rm RJ} = T_\gamma(1 - 2y)$ in the Rayleigh–Jeans part of the spectrum where there are too few photons, and an exponential rise in temperature in the Wien region with too many photons. The magnitude of the distortion is related to the total energy transfer $\Delta E/E = 4y$ where

$$y = \int_0^z \frac{k[T_{\rm e}(z) - T_\gamma(z)]}{m_{\rm e}c^2} \sigma_T n_{\rm e}(z) c \frac{{\rm d}t}{{\rm d}z'}{\rm d}z', \quad (2)$$

is the dimensionless integral of the electron pressure $n_{\rm e}k\,T_{\rm e}$ along the line of sight, $m_{\rm e}$, $n_{\rm e}$ and $T_{\rm e}$ are the electron mass, spatial density, and temperature, T_γ is the photon temperature, k is Boltzmann's constant, z is redshift, and σ_T denotes the Thomson cross section (Sunyaev and Zeldovich, 1970). Energy transfer at higher redshift $10^4 < z < 10^7$ approaches the equilibrium Bose-Einstein distribution, characterized by the dimensionless chemical potential $\mu_0 = 1.4\Delta E/E$. Free-free emission thermalizes the spectrum at long wavelengths. Including this effect, the chemical potential becomes frequency-dependent,

$$\mu(x) = \mu_0 \exp\left(-\frac{2x_{\rm b}}{x}\right), \quad (3)$$

where $x_{\rm b}$ is the transition frequency at which Compton scattering of photons to higher frequencies is balanced by free-free creation of new photons. The resulting spectrum has a sharp drop in brightness temperature at centimeter wavelengths (Burigana et al., 1991).

A chemical potential distortion is a primary signature for the decay of relics from GUT and Planck-era physics. Such relics are expected to exist. Growing evidence points to the existence of "dark matter" observed only through gravitational effects, with density $\Omega_{\rm m} = 0.22^{+0.01}_{-0.02}$ compared to the critical density (Spergel et al., submitted for publication). A leading candidate for dark matter composed of weakly interacting massive particles is the lightest supersymmetric particle χ, the neutralino (Jungman et al., 1996). Neutralinos annihilate primarily into quark-antiquark pairs, which in turn cascade to photons, electrons, positrons, and neutrinos. The annihilation rate $\Gamma = n_\chi n_{\bar\chi}\langle\sigma v\rangle$, where $\langle\sigma v\rangle \sim 6\times10^{-26}\,{\rm cm}^3\,{\rm s}^{-1}$ at freeze out and the neutralino space density n_χ varies as z^3 from the overall

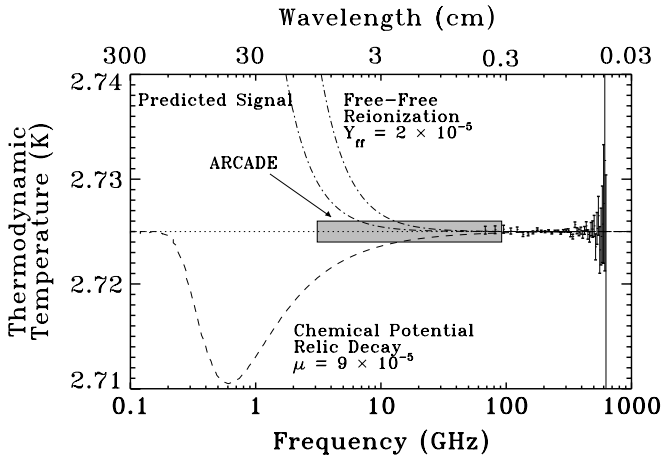

Fig. 2. Current 95% confidence upper limits to distorted CMB spectra, along with the predicted signal from reionization and structure formation. The FIRAS data and ARCADE 1 mK anticipated error box are also shown. ARCADE has both the sensitivity and control of systematic errors to measure the expected signal from the high-redshift universe.

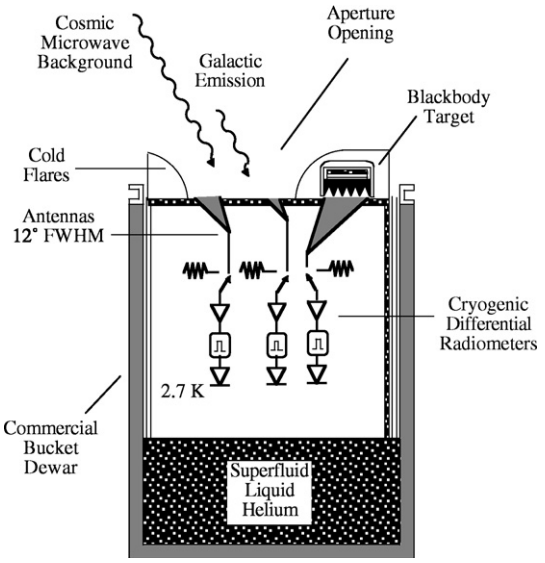

Fig. 3. Schematic drawing of the ARCADE instrument.

expansion of the universe. Gamma radiation from neutralino annihilation in the galactic dark matter halo has been proposed to explain the excess flux observed by the EGRET mission (Fornengo et al., 2004; Valle, 2004). A chemical potential distortion to the CMB spectrum is an inevitable result of neutralino annihilation: annihilations sufficient to produce the EGRET excess would necessarily produce a chemical potential distortion. Measurements of the CMB spectrum can thus provide important constraints on the mass, cross section, and decay modes of dark matter candidates.

Fig. 2 shows current upper limits to spectral distortions at long wavelengths. The CMB spectrum is poorly constrained at centimeter or longer wavelengths, where observable signals from reionization or relic decay are expected to exist. New measurements with mK accuracy can provide important checks for both cosmology and high-energy physics. The absolute radiometer for cosmology, astrophysics, and diffuse emission (ARCADE) is a balloon-borne instrument to provide precisely such new data.

2. Instrument description

ARCADE is a balloon-borne, fully cryogenic, double-nulled instrument to compare the temperature of the sky to a precision on-board blackbody calibrator. Fig. 3 shows a schematic of the instrument. It consists of seven[1] narrow-band cryogenic radiometers ($\Delta\nu/\nu \sim 10\%$) with central frequencies $\nu = 3.3$, 5.5, 8.1, 10, 30, and 90 GHz chosen to cover the gap between full-sky surveys at radio frequencies ($\nu < 3$ GHz) and the FIRAS millimeter and sub-mm measurements ($\nu > 60$ GHz). Each radiometer measures the difference in power between a beam-defining antenna (FWHM 11°.6) and a temperature-controlled internal reference load. An independently controlled blackbody calibrator (emissivity $\epsilon > 0.9999$) is located on the aperture plane, and moves to cover each antenna in turn, so that each antenna alternately views the sky or a known blackbody. The calibrator temperature can be adjusted to null the sky-antenna signal difference. ARCADE thus measures small spectral shifts about a precise blackbody, greatly reducing dependence on instrument calibration and stability. The calibrator, antennas, and radiometer front-end amplifiers are all maintained near thermal equilibrium with the CMB. Boiloff helium vapor, vented through the aperture, forms a barrier between the instrument and the atmosphere, allowing operation in full cryogenic mode and greatly reducing thermal gradients within the instrument.

Fig. 4 shows a block diagram of the ARCADE radiometers. Each radiometer consists of a cryogenic front end with a high electron mobility transistor (HEMT) direct-gain receiver, switched at 75 Hz for gain stability between a wavelength-scaled corrugated conical horn antenna and a temperature-controlled internal load. We switch between the sky horn and internal load using latching ferrite switches (8, 10, 30, and 90 GHz) or coaxial MEMS switches (3 and 5 GHz) maintained near the CMB temperature to reduce effects of insertion loss to negligible levels. The radiometer back ends are housed in a temperature-controlled module mounted outside the dewar, with stainless steel waveguide (30 GHz and above) or coax (10 GHz and below) providing the RF link between the cryogenic and room-temperature components. The back end of each radiometer is split into two frequency sub-channels: one covering the lower half of the front-end passband and an independent channel covering the upper half of the front-end passband. Video

[1] Two independent radiometers operate at 30 GHz, with identical amplification chains but different beam sizes as a cross-check on emission from the reflector hiding the balloon and flight train.

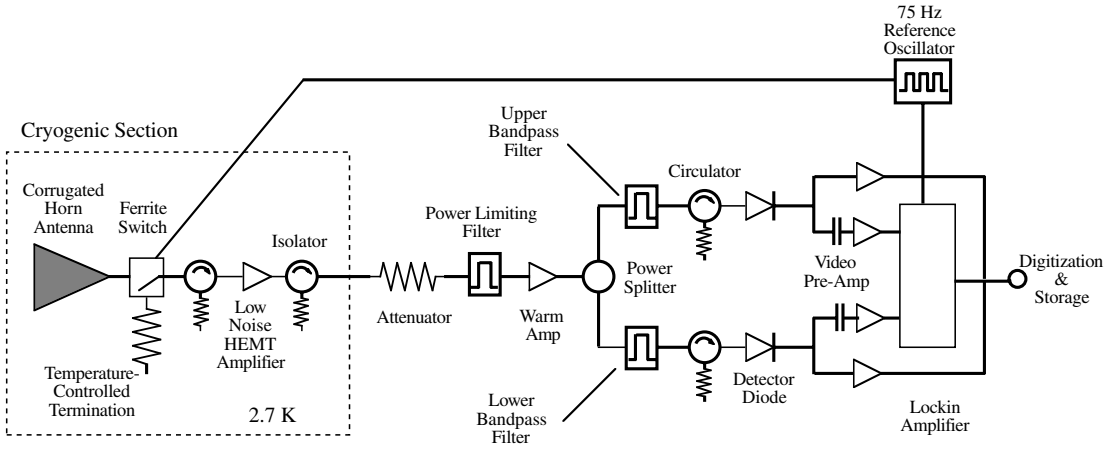

Fig. 4. Block diagram of ARCADE radiometers.

preamplifiers following each detector diode separately amplify the dc and ac portions of the signal, proportional to the total power on the diode and the antenna-load temperature difference, respectively. A lockin amplifier demodulates the switched (ac) signal and integrates for one second to produce an output proportional to the difference in power between the antenna and the internal load. The lockin output and total power signals are digitized at 1 Hz and written to an on-board recorder before being telemetered to the ground.

2.1. Internal loads

The internal reference load has a dual purpose: it provides a stable cold reference for the fast gain chop, and can be adjusted in temperature during flight to eliminate the radiometric offset resulting from imbalance within the switch or between the two arms of the radiometer. An ideal load would have negligible reflection and be isothermal so that its radiometric signal could be computed from a single thermometer connected to the absorbing element. We come close to this ideal using a thin layer of cryogenic-compatible microwave absorber cast inside a copper waveguide. The absorber consists of stainless steel powder mixed with a commercially available epoxy and can be tuned for the desired electromagnetic properties (Wollack et al., submitted for publication-a). The absorber is thermally anchored within a high-thermal-conductivity waveguide, which in turn in surrounded by foam insulation with RF connection through a short stainless steel waveguide section. A resistive heater mounted on a coaxial copper tube surrounding the foam layer provides thermal control, with cooling through a thin copper wire sunk to the 1.55 K liquid helium (LHe) bath. Neither the heater nor the cooling wire are attached directly to the copper waveguide, which acts as an open thermal circuit to minimize thermal gradients across the absorber. We measure power reflection -30 dB or better across the band for each load (Wollack et al., submitted for publication-b). Differential corrections for standing waves are thus reduced below 1 mK for load setpoint changes as large as 1 K.

2.2. External calibrator

The external calibrator provides an absolute radiometric calibration by replacing the sky signal with emission from a blackbody source at a known temperature. Comparison of the sky to the external calibrator provides a second level of nulling in which fixed instrumental signals from internal absorption or reflection will cancel. The calibrator consists of a set of 298 absorbing cones mounted on a thermal diffusion plate and weakly coupled to a liquid helium reservoir (Fig. 5). Fountain-effect pumps lift superfluid liquid helium from the main dewar to the calibrator; thermal control is provided by heaters mounted on the back side of the thermal diffusion plate. The calibrator is mounted within a rotating carousel above the cold aperture plane, and can be moved to cover each antenna in turn.

The calibrator must satisfy several competing design requirements. It must be black (emissivity $e > 0.999$ or reflectivity $r = 1 - e < 0.001$) while maintaining a well-defined temperature. It must completely fill the largest antenna aperture (620 mm diameter) while remaining compact enough to mount at the top of an open bucket dewar. We meet these requirements using a composite design. Each cone within the calibrator is 88 mm tall and consists of an aluminum core coated with a 7 mm absorbing "skin" made from steelcast absorber (Wollack et al., submitted for publication-a). A copper wire extends from the inner aluminum cone into the absorber tip. Together, the aluminum and copper provide a high thermal conductivity path to reduce thermal gradients within each cone, allowing 95% of the absorber volume to remain within 0.5 mK of the base temperature (Fixsen et al., 2006).

The instrument operates in a null mode, with the calibrator temperature close to the sky temperature so that small reflections in the radiometer/calibrator system cancel to first order. Reflections from the calibrator create a systematic offset in the sky-calibrator comparison

$$\Delta T_{\rm cal} = r(T_{\rm sky} - T_{\rm cal}). \quad (4)$$

proportional to the calibrators power reflection coefficient r and the temperature difference between the calibrator and the sky. Requiring $\Delta T_{\rm cal} < 0.1$ mK requires $r < 10^{-3}$. Direct measurements of the antenna-calibrator combination in flight configuration show the power reflection $r < -42$ dB in the worst frequency band (Fixsen et al., 2006). The calibrator completely covers the antenna aperture and is mounted nearly flush with the aperture plane. Measurements of the leakage through the 1 mm gap between the calibrator and the antenna aperture limit spillover past the calibrator to less than -50 dB. Cold flares surrounding the aperture plane redirect any residual spillover to blank areas of the sky. Despite having an absorber less than one wavelength tall, the ARCADE calibrator is demonstrated to be black to better than 0.01% across five octaves in frequency.

2.3. Thermometry

ARCADEs double-null design reduces the problem of precise radiometric photometry to one of simple thermometry: we adjust the temperature of the internal load to produce nearly zero output voltage on the differential radiometer, and then adjust the temperature of the external calibrator until it matches the sky. Provided the radiometer is linear and the emissive components are nearly isothermal, the sky temperature can then be read off from the instrument thermometry.

We monitor cryogenic temperatures using four-wire ac resistance measurements of 120 ruthenium oxide thermometers read out every 1.067 s (Fixsen, 2002). Twenty six of the thermometers are embedded in the absorbing skin of selected cones within the external calibrator. An additional nine thermometers measure temperatures on the calibrator diffusion plate, liquid helium tank, and surrounding support structures. Twenty one additional thermometers monitor three critical temperatures (antenna throat, internal load, and the Dicke switch/cryogenic HEMT amplifier) on each of the seven radiometers. The remaining thermometers monitor the temperature of the aperture plane, cold flares, superfluid pumps, liquid helium reservoirs (main tank, external calibrator, aperture plane, and radiometer bases) as well as the dewar walls and the instrument support structure inside the dewar.

The in-flight thermometry compares the resistance of each thermometer to a set of four calibration resistors spanning the dynamic range of the thermometer resistances. The calibration resistors are part of the readout electronics board, located in a temperature-controlled enclosure. One of the calibration resistors includes the electrical harness into the dewar to monitor possible effects from electrical pickup or stray capacitance. The flight software uses a lookup table to infer a temperature for each thermometer using temperature–resistance curves derived from ground tests.

The instrument is mainly a transfer standard to compare the sky to the external calibrator; precise knowledge of the absolute temperature is required only for the external calibrator. We build low-mass ruthenium oxide resistance thermometers and establish the resistance to temperature calibration for each thermometer in the external calibrator by measuring the resistance of the embedded thermometers while stepping the temperature of the instrumented cones from 1.3 K to 15 K. A separate NIST-calibrated resistance thermometer of identical design monitors the temperature throughout the calibration to transfer the NIST calibration to the flight thermometers. Since the thermometers are calibrated in situ, the small self-heating is inherently included. This calibration has proved to be stable with respect to time. Observations of the superfluid helium transition at 2.1768 K are easlily observable in the calibration data

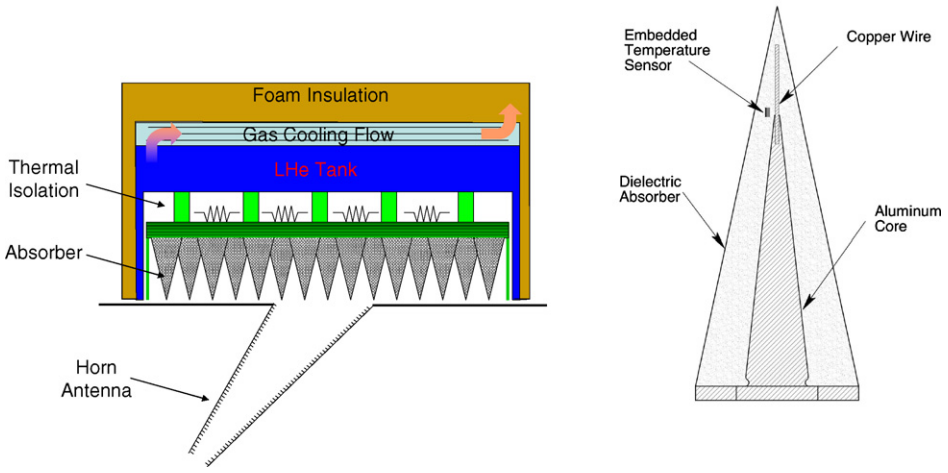

Fig. 5. Schematic of ARCADE external calibrator. (Left) An array of conical microwave absorbers is weakly coupled to a superfluid LHe reservoir. Liquid-filled "wings" on the reservoir intercept potential heat leaks from outside the dewar. A metal/fiberglass thermal diffusion plate serves to reduce the thermal "footprint" of heaters at the absorber. (Right) A single absorbing cone consists of a metal core covered by microwave absorber. Thermometers embedded within the absorber monitor the temperature of the calibrator.

and provide a convenient cross-check on the resistance-temperature calibration. The calibration is stable within 0.3 mK across eight independent calibrations over four years, providing both a cross-check on the absolute thermometry and a limit to possible systematic drifts in the thermometer resistance-to-temperature curves (Kogut, 2004).

2.4. Antennas

Each receiver is fed by a corrugated conical horn antenna scaled in wavelength to produce identical 11°.6 full width at half maximum beam shape in each frequency channel. To avoid convective instabilities in the helium vapor barrier, the instrument should remain vertical during observations. We reconcile this requirement with the need for sky coverage (and avoiding direct view of the balloon) by mounting the antennas at a 30° angle from the zenith, slicing each antenna at the aperture plane. The slice has minimal effect on the symmetry of the beams (Singal, 2005).

2.5. Dewar and cryogenic aperture

Active thermal control maintains the external calibrator, antennas, Dicke switches, and front-end amplifiers at temperatures near 2.7 K, in thermal equilibrium with the CMB signal. To avoid correction for beam spillover onto the dewar walls, we mount the antennas at the top of an open bucket dewar 1.5 m in diameter and 1.8 m deep. We further avoid corrections for emission or reflection from a window over the cold optics by using an open aperture with no window between the cryogenic aperture and the ambient environment. Boiloff helium vapor, vented through the aperture, forms a barrier between the instrument and the atmosphere to allow operation in fully cryogenic mode.

Previous flights validate the open-aperture design. The efflux of helium gas above the aperture (roughly 5 m^3 s^{-1} at 35 km float altitude) does not completely eliminate condensation of atmospheric nitrogen onto the cryogenic optics, but does reduce it to levels compatible with the desired CMB observations. Data from a 2001 flight of a two-channel prototype payload show excess heat dissipation on the aperture plane, consistent with an accumulation rate of approximately 200 g hr^{-1} of nitrogen onto the aperture, a heat source of order 6 W (Kogut, 2004). Visual examination using an on-board video camera confirms this slow accumulation of nitrogen ice, with several mm of "frost" visible on the optics an hour after opening the ascent lid (Fig. 6). Nitrogen ice is nearly transparent at cm wavelengths. Since the ice cools to the same temperature as the rest of the optics, modest accumulations affect only mechanical operations. Analysis of the 2003 and 2005 flight data shows no detectable radiometric signal from ice accumulation (Fixsen, 2004; Singal et al., 2006).

ARCADE has a large (kW) heater on the cold optics to allow periodic de-icing of the external calibrator, antenna aperture, and horn throat sections. With the superfluid pumps off, the aperture plane and calibrator have only weak thermal coupling to the dewar. Raising the aperture plane and calibrator above 80 K for 15 m suffices to remove accumulated nitrogen ice with only a modest impact on the main liquid helium reservoir. Atmospheric condensation is not a limiting problem.

3. Instrument status

ARCADE was first selected for development in December 1999. Flights of a two-channel prototype in November 2001 and June 2003 demonstrated that a large (45 cm diameter) instrument can be maintained at 2.7 K at the top of a bucket dewar without windows between the cold optics and the atmosphere (Fixsen, 2004; Kogut, 2004). Based on this experience, a larger six-channel instrument flew in July 2005. This second-generation instrument extended the frequency coverage to the longer wavelengths needed to reach the main science goals, while incorporating improvements in the cryogenic engineering suggested by the first-generation instrument. A gearbox mechanical failure during the 2005 flight allowed only one antenna to view the sky, sharply limiting the potential science return. Engineering data showed that the remainder of the instrument,

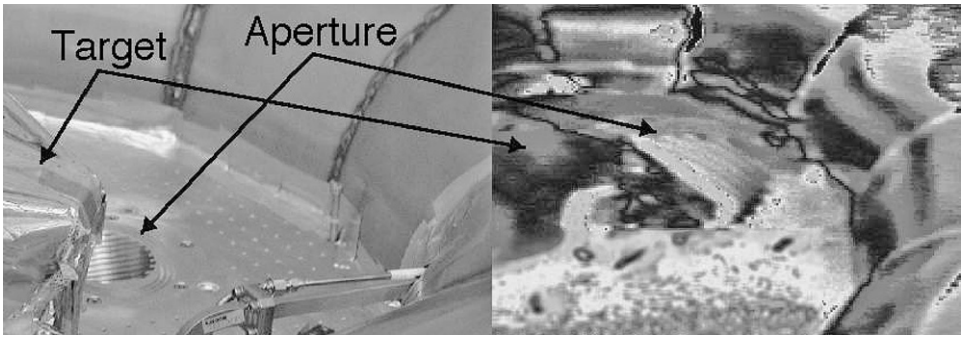

Fig. 6. Aperture plane from 2001 flight with calibrator and antenna aperture. (left) 30 GHz aperture during ground testing. The calibrator is visible in the left foreground; the cold flares are in the background. (right) video still taken during 2001 flight, 30 m after opening ascent lid. The corrugations of the 10 GHz aperture are visible behind the calibrator in the foreground – nitrogen condensation is not a major problem.

including the radiometers and external calibrator, performed well, demonstrating the basic functionality of the second-generation instrument.

Science data from the 2005 flight include several hours of sky data with the 8 GHz radiometer, operated in single-null condition without the ability to view the external calibrator. Even without the absolute reference, the radiometer is sufficiently stable and linear to allow a measurement of the CMB temperature and galactic foreground emission, albeit at somewhat degraded accuracy (Singal et al., 2006). We have since modified payload to prevent a recurrence and will re-fly the modified payload in July 2006.

The ARCADE design minimizes most sources of systematic error. The leading uncertainty from the 2006 flight is expected to result from small thermal gradients in the calibrator as heat flows from the calibrator back plate through the absorber to the colder aperture plane below. Future flights will reduce this source of uncertainty by modifying the cryogenic aperture to allow active thermal control of the aperture plate and antenna mount structure. The metal plate mounting the antenna apertures is large (nearly 2 m^2 area) and exposed, with complicated interactions through turbulent gas layers to both the liquid helium below and the ambient atmosphere above. The large efflux of helium gas precludes ground tests in a thermal vacuum chamber, requiring actual flight data to allow engineering of incremental improvements. A series of engineering tests during the 2006 flight will provide thermal data to guide modifications to the aperture plane allowing active thermal control for a flight in 2007.

References

Bartlett, J.G., Stebbins, A., 1991. ApJ 371, 8.
Burigana, C., Danese, L., De Zotti, G.F., 1991. A&A 246, 49.
Burigana, C., De Zotti, G.F., Danese, L., 1995. A&A 303, 323.
Fixsen, D.J. et al., 2002. RSI 73, 3659.
Fixsen, D.J. et al., 2004. ApJ 612, 86.
Fixsen, D.J., Mather, J.C., 2002. ApJ 581, 817.
Fixsen, D.J. et al., 2006. RSI 77, 064905.
Fornengo, N., Pieri, L., Scope, S., 2004. PRD 70, 103529.
Gnedin, N.Y., Ostriker, J.P., 1997. ApJ 486, 581.
Gush, H.P., Halpern, M., Wishnow, E.H., 1990. PRL 65, 537.
Haiman, Z., Loeb, A., 1997. ApJ 483, 21.
Jungman, G., Kamionkowski, M., Griest, K., 1996. PhR 267, 195.
Kogut, A. et al., 2004. RSI 75, 5079.
Kogut, A. et al., 2004. ApJS 154, 493.
Mather, J.C. et al., 1990. ApJ 354, L37.
Oh, S.P., 1999. ApJ 527, 16.
Singal, J. et al., 2005. RSI 76, 124703.
Singal, J., et al., 2006. ApJ, in press.
Spergel, D.N., et al., ApJ, submitted for publication (preprint astro-ph/0603449).
Sunyaev, R.A., Zeldovich, Ya.B., 1970. Ap&SS 7, 20.
Valle, G., 2004. A&A 424, 765.
Wollack, E., et al., submitted for publication-a. Applied Optics.
Wollack, E., et al., submitted for publication-b. IEEE transactions on instrumentation and measurement.
Zeldovich, Ya.B., Sunyaev, R.A., 1969. Ap&SS 4, 301.